OXFORD

SOT | Society of Toxicology
www.toxsci.oxfordjournals.org

TOXICOLOGICAL SCIENCES, 157(2), 2017, 438–450

doi: 10.1093/toxsci/kfx055
Advance Access Publication Date: April 11, 2017
Research article

Predicting Transport of 3,5,6-Trichloro-2-Pyridinol Into Saliva Using a Combination Experimental and Computational Approach

Jordan Ned Smith,[1] Zana A. Carver, Thomas J. Weber, and Charles Timchalk

Health Impacts and Exposure Science, Pacific Northwest National Laboratory (PNNL), Richland, Washington 99352

[1]To whom correspondence should be addressed. Fax: (509) 376-9064. E-mail: jordan.smith@pnnl.gov.

ABSTRACT

A combination experimental and computational approach was developed to predict chemical transport into saliva. A serous-acinar chemical transport assay was established to measure chemical transport with nonphysiological (standard cell culture medium) and physiological (using surrogate plasma and saliva medium) conditions using 3,5,6-trichloro-2-pyridinol (TCPy) a metabolite of the pesticide chlorpyrifos. High levels of TCPy protein binding were observed in cell culture medium and rat plasma resulting in different TCPy transport behaviors in the 2 experimental conditions. In the nonphysiological transport experiment, TCPy reached equilibrium at equivalent concentrations in apical and basolateral chambers. At higher TCPy doses, increased unbound TCPy was observed, and TCPy concentrations in apical and basolateral chambers reached equilibrium faster than lower doses, suggesting only unbound TCPy is able to cross the cellular monolayer. In the physiological experiment, TCPy transport was slower than nonphysiological conditions, and equilibrium was achieved at different concentrations in apical and basolateral chambers at a comparable ratio (0.034) to what was previously measured in rats dosed with TCPy (saliva:blood ratio: 0.049). A cellular transport computational model was developed based on TCPy protein binding kinetics and simulated all transport experiments reasonably well using different permeability coefficients for the 2 experimental conditions (1.14 vs 0.4 cm/h for nonphysiological and physiological experiments, respectively). The computational model was integrated into a physiologically based pharmacokinetic model and accurately predicted TCPy concentrations in saliva of rats dosed with TCPy. Overall, this study demonstrates an approach to predict chemical transport in saliva, potentially increasing the utility of salivary biomonitoring in the future.

Key words: biomonitoring, alternatives to animal testing; *in vitro* and alternatives, biological modeling, exposure assessment; risk assessment.

The National Research Council of the National Academies report, *Exposure Science in the 21st Century: A Vision and a Strategy* (2012), called for an extensive expansion of human and ecological exposure assessment. Understanding the relationship between a stressor and a receptor is fundamental in many disciplines including toxicology, epidemiology, environmental regulation, environmental planning, and disaster management (2012). Quality human exposure data are paramount to successfully implementing new concepts such as the Aggregate Exposure Pathway framework which promotes integration of exposure science in risk-based decisions of public health (Teeguarden *et al.*, 2016).

Biomonitoring techniques have become valuable tools for quantitatively evaluating human exposures to chemicals from both occupational and environmental sources. Direct measurement of chemical exposures provides the most accurate estimation of actual exposures (Nieuwenhuijsen *et al.*, 2006), and noninvasive matrices (eg, saliva) have been advocated over traditional matrices (eg, blood) to facilitate ease of sample collection, maximize volunteer participation, and potentially reduce cost (Kaufman and Lamster, 2002; Nigg and Wade, 1992). A number of biomarkers have been found in saliva, and many of these have been evaluated as potential noninvasive biomonitoring candidates (Kaufman and Lamster, 2002; Lu *et al.*, 1997, 2003; Michalke *et al.*, 2015; Smith *et al.*, 2010, 2012; Timchalk *et al.*, 2007). Using saliva as a biomonitoring matrix has potential to significantly advance quantitative dosimetry as an integral

component of biomonitoring efforts; however, the inability to predict which chemicals are readily cleared in saliva at levels that can be quantified from occupationally relevant exposure levels remains a major limitation (Michalke *et al.*, 2015). Additionally, consistent quantitative relationships between saliva and blood remain difficult to obtain and unknown for many chemicals (Michalke *et al.*, 2015).

Chemical compounds can transfer from blood to saliva by passive transcellular diffusion, active transcellular transport, or paracellular ultrafiltration through tight junctions (Haeckel, 1993; Jusko and Milsap, 1993). Generally, passive transcellular diffusion is thought to be the primary method for which most chemicals are transferred from blood to saliva. Physicochemical properties that affect the amount of diffusion across a concentration gradient from blood to saliva include molecular size, lipid solubility, the dissociation constant of ionized compounds, and extent of plasma-protein binding (Haeckel, 1993; Jusko and Milsap, 1993). Passive diffusion from blood to saliva has previously been predicted using partitioning algorithms (Schmitt, 2008; Smith *et al.*, 2010, 2012; Timchalk *et al.*, 2015); however, *in silico* predictions are rarely a valid replacement for quality experimental data where mechanisms can be directly measured, such as protein binding or active transport.

In order to identify chemicals that can transport into saliva, a salivary gland epithelial cell system has recently been developed as a screening platform to detect chemicals that can be cleared through an epithelial barrier (Weber *et al.*, 2017). Primary rat serous-acinar cells were isolated from the submaxillary gland and defined by alpha amylase and aquaporin-5 expression (Weber *et al.*, 2017). Primary rat serous-acinar cells form extensive tight junctions that can tolerate moderate stress without loss of barrier function when cultured on Transwell membranes (Weber *et al.*, 2017). Serous-acinar barrier function and chemical transport was demonstrated using lucifer yellow (a cell impermeable compound) and chlorpyrifos (an organophosphate pesticide) (Weber *et al.*, 2017). Because of these characteristics, primary serous-acinar cells are an excellent platform to investigate chemical transport *in vitro*. Computational models can be used as a tool to better interpret mechanistic transport of chemicals in the serous-acinar model system and can be used to extrapolate *in vitro* results to human predictions.

The objective of this study was to develop an experimental and computational approach to predict chemical transport into saliva, which requires developing a computational model of the serous-acinar chemical transport assay. Previously, other cellular transport computational models have been used to interpret chemical transport data using a mechanistic approach (Poirier *et al.*, 2008). With our goal of extrapolating *in vitro* experiments to *in vivo* predictions, the computational model developed here focused on mechanistic transport of chemicals in the serous-acinar chemical transport assay. Our group has previously evaluated *in vivo* pharmacokinetics of pesticide transport into saliva with rats (Smith *et al.*, 2010, 2012). We have also developed physiologically based pharmacokinetic (PBPK) models of pesticide transport (Smith *et al.*, 2010, 2012; Timchalk *et al.*, 2015). By maintaining mechanistic descriptions of serous-acinar chemical transport, parameters from the computational model may have relevance for *in vivo* extrapolation utilizing techniques such as PBPK modeling. In this study, *in vitro* transport of the chlorpyrifos metabolite 3,5,6-trichloro-2-pyridinol (TCPy) was measured using nonphysiological and physiological transport experiments with the serous-acinar chemical transport assay. A computational model was developed to interpret *in vitro* TCPy transport experiments and was integrated into a PBPK model to predict *in vivo* levels of TCPy in rat saliva.

MATERIALS AND METHODS

Chemicals. TCPy and TCPy-$^{13}C_2$-^{15}N (stable isotope TCPy) were kindly provided by the Dow Chemical Company (Midland, Michigan, USA). The TCPy stable isotope had ^{13}C located at the 2 and 6 positions and the ^{15}N located at the 1 position of the pyridinol ring. N-(tert-butyldimethylsilyl)-N-methyltrifluoroacetamide (MTBSTFA), ethyl acetate, toluene, lucifer yellow, and other general laboratory chemicals were purchased from Sigma-Aldrich (St Louis, Missouri, USA).

TCPy protein binding. Levels of TCPy binding to protein was measured in cell culture medium and rat plasma. TCPy was spiked into cell culture medium (Advanced DMEM:F12 with 2% FBS) at 6 different concentrations (9–1300 μM), diluted (1.6% in PBS) cell culture medium with additional bovine serum albumin used in the physiological transport experiment (see "Physiological Transport Experiment" section) at 9 different concentrations (24–1020 μM), or diluted rat plasma (3% in PBS) at 5 different concentrations (35–760 μM). Samples were incubated at 37°C for 1 h, and aliquots of each sample were transferred to Amicon Ultra Centrifugal Filters (10 kDa molecular weight cutoff). Samples were centrifuged for 20 min at 14 000 relative centrifugal force (RCF) ×g. TCPy concentrations in unfiltered solutions and filtrate were quantified using gas chromatography-mass spectrometry (GC-MS) (see "TCPy Quantification" section). Bound TCPy concentrations (C_b, calculated by difference of total and unbound TCPy concentrations) were evaluated as a function of unbound TCPy concentrations (C_u) using 2 nonlinear models. The first model describes TCPy protein binding assuming 1 apparent-binding site, where B_{max} is the maximum number of binding sites and k_d is the affinity constant (Equation 1). The second model assumes 2 apparent binding sites, where B_{max1} and B_{max2} are the maximum number of binding sites and k_{d1} and k_{d2} are affinity constants (Equation 2). Both models were optimized using a maximum likelihood objective. The Bayesian information criterion (BIC), which includes a penalty for model complexity, was used to judge the best-fit model for evaluating TCPy protein binding. Protein concentrations were measured using bicinchoninic acid assay (BCA) and bovine serum albumin as an external standard.

$$C_b = \frac{Bmax \times C_u}{k_d + C_u} \quad (1)$$

$$C_b = \frac{Bmax_1 \times C_u}{k_{d1} + C_u} + \frac{Bmax_2 \times C_u}{k_{d2} + C_u} \quad (2)$$

Cell culture. Primary serous-acinar cells were isolated from adult male Sprague Dawley rat submaxillary glands. Cells were characterized by alpha amylase and aquaporin 5 expression as previously described in Weber *et al.* (2017). Serous-acinar cells were maintained in Advanced DMEM:F12 supplemented with 2% FBS, 2 mM GlutaMAXTM, 10 ng/ml epidermal growth factor and standard antibiotics/antimycotics (100 U/ml penicillin, 100 U/ml streptomycin, and 0.25 μg/ml Fungizone). Cells were subcultured by trypsinization (0.25%).

Serous-acinar chemical transport assay. Chemical transport was measured using serous-acinar chemical transport assay. Serous-acinar cells were seeded on Falcon Transwell inserts

(3 μm pore, 2.0 ± 0.2 × 105 pores/cm^2, 6-well plate). High pore density membranes were selected to promote maximal rates of diffusion across the Transwell insert. Cells were used for chemical transport studies when sufficient tight junctions had formed as previously defined (Weber *et al.*, 2017). Transepithelial electrical resistance (TEER) used as a measure of tight junction formation and was measured using the EVOM2 and Endohm 24-SNAP system (World Precision Instruments, Sarasota, Florida, USA). TEER values $\geq$ 656 Ω × cm^2 are associated with passage of < 1% lucifer yellow/hour across the epithelial barrier, which is adequate for chemical transport studies (Weber *et al.*, 2017). In practice, TEER values routinely reached values ranging between 1852 and 4287 Ω × cm^2, which enabled cells to tolerate moderate stress responses without loss of barrier function. During each experiment, lucifer yellow passage was measured concurrently with analyte transport as an "internal standard" of tight junction integrity (Weber *et al.*, 2017). The chamber receiving the analyte dose was spiked with 25 μg/ml lucifer yellow at the beginning of each experiment, and the contralateral chamber was sampled at various time points. Lucifer yellow was quantified in medium from the contralateral chamber with a fluorescence microplate reader (Cytofluor 4000, Perseptive Biosystems, Framingham, Massachsetts, USA) using 450/50 and 530/25 excitation/emission filters sets, respectively. Once tight junctions were formed and verified with TEER, either a nonphysiological or a physiological transport experiment was conducted as described below.

Nonphysiological transport experiment. The nonphysiological transport experiment utilized serous-acinar cells grown on Transwell inserts using normal cell culture medium (Advanced DMEM:F12 with 2% FBS) in apical and basolateral chambers. Once tight junctions were formed (approximately 7 days), media in both chambers was changed, cultures were allowed to equilibrate (approximately 1 h). At the time of medium change, the basolateral chamber received 1 ml of fresh medium, while the apical chamber received 2 ml of medium. After equilibration, TCPy was administered at 2× the nominal dose concentration (1 ml) to the existing medium (1 ml), resulting in 2 ml total volume and 1× the nominal dose concentration in the basolateral chamber. Cells were dosed with 13–140 μM TCPy. Medium from both chambers was sampled (200 μl) repeated at 2, 4, 6, 8, and 24 h. Cells were harvested at 8 and 24 h. TCPy was quantified in sampled medium and cells. Lucifer yellow was quantified in medium at 24 h.

Physiological transport experiment. In order to simulate physiologically relevant chemical transport, protein concentrations of cell culture medium in the apical and basolateral chambers were modified to simulate those found in plasma and saliva. Reported protein concentrations for saliva and plasma were 3 and 54–65 mg/ml, respectively, for a plasma:saliva ratio of approximately 20 in rats (Hold *et al.*, 1995; Ritschel and Tompson, 1983; Zaias *et al.*, 2009). Two physiological transport experiments were conducted: (1) using the same relative protein concentration ratio found in plasma and saliva (1.3 and 27 mg/ml, respectively), and (2) using absolute protein concentrations found in plasma and saliva (2.5 and 52 mg/ml, respectively).

For the relative physiological transport experiment, cells were seeded on Transwell inserts, tight junctions were allowed to form, and medium was changed prior to dosing. Apical medium (saliva surrogate) consisted of Advanced DMEM:F12 (1.3 mg/ml total protein) and basolateral medium (plasma surrogate) consisted of Advanced DMEM:F12 with 2% FBS supplemented with bovine serum albumin (27 mg/ml total protein). As with the nonphysiological transport experiment, 1 ml of 2× nominal dosing concentration was added to the basolateral chamber. The TCPy dosing concentration was higher (300 μM) in the physiological transport experiment than the nonphysiological transport experiment to ensure sufficient analytical sensitivity for measuring TCPy in the apical medium. Medium was sampled from the apical and basolateral chambers at 2, 4, 8, and 24 h.

The procedure for the absolute physiological transport experiment was identical to the relative physiological transport experiment, except the apical medium (saliva surrogate) consisted of Advanced DMEM:F12 containing 2% FBS and supplemented bovine serum albumin (2.5 mg/ml total protein) and the basolateral chamber (plasma surrogate) had more bovine serum albumin (52 mg/ml). Medium was sampled from the apical and basolateral chambers at 8, 24, and 32 h.

TCPy quantification. TCPy was extracted from cell culture medium and cells using liquid-liquid extraction and quantified using GC-MS (Brzak *et al.*, 1998). Briefly, a stable TCPy isotope was added to each sample as an internal standard (2.5 nmol). Samples were acidified using 3 M HCl saturated with NaCl. Analytes were extracted twice using ethyl acetate. Extracts were dried with Na_2SO_4 and evaporated under a gentle stream of nitrogen. Residues were reconstituted with toluene and derivatized with MTBSTFA. An external calibration curve was prepared simultaneously by spiking known amounts of TCPy into control medium or cells and extracting those samples using the same method. Samples were analyzed using a Hewlett-Packard (Palo Alto, California, USA) 5973B mass selective detector in negative ion chemical ionization mode interfaced with Hewlett-Packard model 6890 GC using ChemStation software for programming and data analysis. Separations were achieved using a Restek (Bellefonte, Pennsylvania, USA) RTX-1701 30 m × 0.25 mm id × 0.25 μm df column. Helium carrier gas was maintained at a constant pressure of 10 psi. GC oven temperature program initiated at 150°C for 1 min followed by a 25°C/min ramp to 180°C, a 20°ramp to 250°C, and was held for 12 min. Inlet temperature was 210°C. Selected ion monitoring (SIM) was used for analysis for increased sensitivity. Ions selected for monitoring included 161 and 166 m/z for the MTBSTFA-TCPy derivative and the MTBSTFA-TCPy internal standard derivative, respectively. Contributions MTBSTFA-TCPy isotope derivative to 161 m/z, and the MTBSTFA-TCPy derivative to 166 m/z ion were corrected (Brzak *et al.*, 1998). The entire method allowed quantification of at least 1.3 μM TCPy.

Cellular transport computational model. A cellular transport computational model was developed to describe chemical transport from the serous-acinar assay. The model describes time course of chemical disposition in the Transwell system among 3 different compartments including apical cell culture medium (No. 1, top chamber), cells (No. 2), and basolateral cell culture medium (No. 3, the bottom chamber) (Figure 1). Transport among compartments was modeled as passive diffusion using ordinary differential equations. Evidence of active transport was not observed in any of the transport experiments, thus modeling efforts focused on diffusion. Diffusion transport was described as a modification to Fick's Law of Diffusion, where t is time (h), A is the amount (nmol), PA is the permeability coefficient (cm/h), SA is the surface area of cells (cm^2), C is concentration (nmol/ml), and P is the partition coefficient (Equations 3–5). The permeability

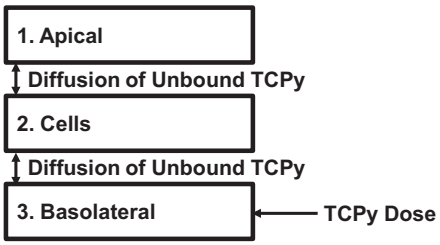

FIG. 1. A computational model for TCPy transport experiments with a serous-acinar chemical transport assay. The computational model consisted of 3 compartments: The apical cell culture medium chamber, the mono layer of serous-acinar cells grown on Transwell inserts, and the basolateral cell culture medium chamber. Transport of TCPy not bound to proteins was modeled using modified Fick's Diffusion.

coefficient is defined as the product of the diffusion coefficient (cm^2/h) and the thickness of the cell membrane (cm).

$$\frac{dA_1}{dt} = -PA_{12} \times SA_2 \times \left(C_1 - \frac{C_2}{P_{21}}\right) \quad (3)$$

$$\frac{dA_2}{dt} = PA_{12} \times SA_2 \times \left(C_1 - \frac{C_2}{P_{21}}\right) + PA_{32} \times SA_2 \times \left(C_3 - \frac{C_2}{P_{23}}\right) \quad (4)$$

$$\frac{dA_3}{dt} = -PA_{32} \times SA_2 \times \left(C_3 - \frac{C_2}{P_{23}}\right) \quad (5)$$

Due to high levels of observed protein binding, unbound and bound TCPy were modeled in apical and basolateral chambers, and only unbound TCPy was allowed to diffuse to the cellular compartment. Protein-binding kinetics was described using ordinary differential equations describing ligand-protein formation as a second order rate and ligand-protein dissociation as a first order rate, where A_u is the amount of unbound TCPy, k_{on} is the second order rate constant of ligand-protein formation, C_u is the concentration of unbound TCPy, C_{bs} is the concentration of unoccupied binding sites, k_{off} is the first order ligand-protein dissociation rate constant, C_b is the concentration of bound TCPy, and V_x is the volume of the compartment (Equation 6). The ratio of k_{dis}/k_{form} is equivalent to the affinity constant (k_d) measured in protein binding experiments. The equation describing the change of the amount of TCPy bound to proteins (Equation 7) is the negative product of the equation describing the change of the amount of TCPy unbound to proteins (Equation 6). The equation describing the change in the amount of unoccupied binding sites (Equation 8) is the same as the equation describing the change of the amount of TCPy unbound to proteins (Equation 6), except the starting value was the total amount of binding sites in each compartment. As such, TCPy starting concentrations were all modeled as unbound at the beginning of each simulation.

$$\frac{dA_u}{dt} = (-k_{on} \times C_u \times C_{bs} + k_{off} \times C_b) \times V_x \quad (6)$$

$$\frac{dA_b}{dt} = (k_{on} \times C_u \times C_{bs} - k_{off} \times C_b) \times V_x \quad (7)$$

$$\frac{dA_{bs}}{dt} = (-k_{on} \times C_u \times C_{bs} + k_{off} \times C_b) \times V_x \quad (8)$$

Parameterization. Parameters within the cellular transport computational model were obtained from literature sources or measured from experiments conducted here. Compartment volumes, surface area of the cells, and thickness of the cellular membrane were defined in the cellular experiments or from literature sources (Table 1). Protein binding parameters were measured (see "TCPy Protein Binding" section). Partition coefficients for TCPy simulations were measured in the nonphysiological transport experiment (240 μM), and permeation coefficients were optimized to TCPy concentrations in medium from apical and basolateral chambers in nonphysiological and physiological transport experiments.

PBPK model. A PBPK model for chlorpyrifos that predicted TCPy salivary excretion in rats and humans (Smith *et al.*, 2010, 2012; Timchalk *et al.*, 2002) was modified to accommodate the cellular transport computational model developed here. Overall, the goal of the modified PBPK model was to maintain the existing PBPK structure and parameters but include the cellular transport computational model developed here for salivary predications. In the chlorpyrifos PBPK model, the disposition of TCPy is described as a one compartment pharmacokinetic model, and saliva concentrations were calculated using a partition coefficient (Smith *et al.*, 2010, 2012; Timchalk *et al.*, 2002). Here, the TCPy volume of distribution compartment was expanded to include blood, blood in salivary glands, salivary glands, saliva, and the rest of the body (Figure 2). This structure allowed the description of TCPy disposition between blood in salivary glands, salivary glands, and saliva to be analogous to the cellular transport computational model with the exception that blood in salivary glands is flowing (Equation 9). In contrast, the basolateral compartment is static in the serous-acinar chemical transport assay. The blood compartment was divided into bound and unbound TCPy. Mathematical descriptions of TCPy protein binding were identical to the bound/unbound description found in the computational cellular transport model (Equation 9). TCPy moved between the unbound blood and the rest-of-body compartments as a flow-limited process. TCPy was absorbed into blood from intravenous or oral routes of exposure or from TCPy formation via chlorpyrifos or chlorpyrifos-oxon metabolism from the existing PBPK model (Smith *et al.*, 2010, 2012; Timchalk *et al.*, 2002). In order to maintain a consistent one compartment description for TCPy, the volume of rest-of-body compartment was defined as the TCPy volume of distribution less blood and salivary gland volumes. TCPy was eliminated from the rest-of-body compartment using existing first order elimination and phase II metabolism rates (Smith *et al.*, 2010, 2012; Timchalk *et al.*, 2002). With the exception of the TCPy model structure change, the PBPK model maintained the same parameters and structure as previously described (Smith *et al.*, 2010, 2012; Timchalk *et al.*, 2002).

$$\frac{dA_{SGBl}}{dt} = Q_{Sg} \times (C_a - C_{vsg}) - PA \times SA_{sg} \times \left(C_{vsg} - \frac{C_{sg}}{P}\right) \quad (9)$$

Sensitivity analysis. Local sensitivity analyses were performed to identify the most important parameters for predicting TCPy transport using the cellular transport computational model and the PBPK model. Normalized sensitivity coefficients were calculated for a 1% change in a given model parameter when all other parameters were held fixed. For the cellular transport computational model, sensitivity analyses were performed in respect of TCPy concentrations in the apical (nondosed) and basolateral (dosed) chambers following both nonphysiological and

TABLE 1. Parameters Used in the Cellular Transport Computational Model for Simulating the Nonphysiological and Physiological Transport Experiments in Serous-acinar Cells

Parameter	Value	References
Volumes (ml)		
Apical chamber	2	Set experimentally
Basolateral chamber	2	Set experimentally
Cells	0.0022	Estimated: (2×10^6 cells) × (1100 μm^3/cell)
Cell Parameters		
Effective Surface area (cm^2)	4.2	Transwell effective growth area
Permeation coeffcient (cm/h) for nonphysiological	1.14	Optimized
Permeation coeffcient (cm/h) for phyisological	0.41	Optimized
Partition Coeffcients (unitless)		
$P_{unbound\ in\ media:cells}$ TCPy	24	Measured
Protein-binding Parameters		
B_{max} (nmol/mg protein) for nonphysiological	123.5	Measured
B_{max1} (nmol/mg protein) for physiological	59.0	Measured
B_{max2} (nmol/mg protein) for physiological	90.6	Measured
K_d (μM) for nonphysiological	30.7	Measured
K_{d1} (μM) for physiological	6.3	Measured
K_{d2} (μM) for physiological	77.2	Measured
K_{on} (1/M/s)	1×10^6	Estimated (Schlosshauer and Baker, 2004; Schreiber *et al.*, 2009; Mironov *et al.*, 2011)
Protein Concentrations		
Nonphysiological transport medium (mg/ml)	1.84	Measured
Physiological plamsa surrogate medium 1 (mg/ml)	27.2	Measured
Physiological saliva surrogate medium 1 (mg/ml)	1.28	Measured
Physiological plamsa surrogate medium 2 (mg/ml)	52.3	Measured
Physiological saliva surrogate medium 2 (mg/ml)	2.51	Measured

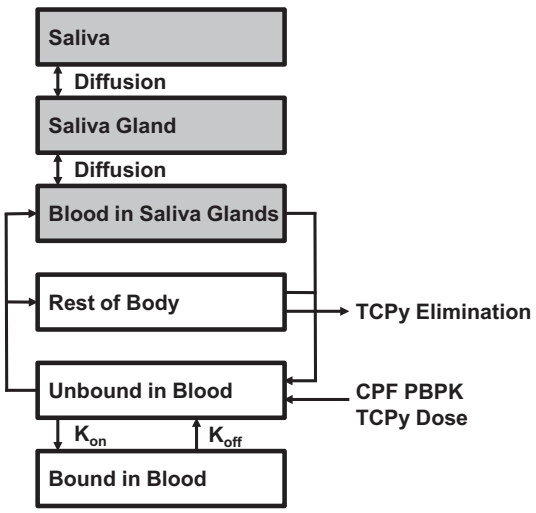

FIG. 2. A modified PBPK model of TCPy disposition. The original one compartment model for TCPy (Timchalk *et al.*, 2002) was expanded to include bound and unbound TCPy in blood, blood in saliva glands, saliva glands, saliva, and rest-of-body compartments. The shaded compartments are analogous to the cellular transport computational model (Figure 1).

physiological transport experiments. Starting TCPy concentrations in the basolateral chambers were 10 and 100 μM. All parameters in the cellular transport computational model were subjected to sensitivity analysis. For the PBPK model, parameters extrapolated from the cellular transport computational model were subjected to a sensitivity analysis in respect to TCPy concentrations in saliva and blood of rats following an iv administration of TCPy (1 mg/kg).

Calculations, statistics, and model coding. The cellular transport computational model and PBPK model were coded in acslXtreme 3.0.2.1 (Aegis Technology, Huntsville, Alabama, USA). Optimizations of model parameters were also conducted using acslXtreme using the Quasi-Newton algorithm using a heteroscedasticity value of 1.0. Initial values were set by adjusting parameters visually, then bounding parameters with reasonable values for optimization. All optimized values were within the initial set bounding range. R: A language and environment for statistical computing, version 2.13.1 (R Foundation for Statistical Computing, Vienna, Austria) was used for protein binding calculations, *t* tests for comparing TCPy concentrations in apical and basolateral chambers, lucifer yellow transport comparisons, and general data analysis.

RESULTS

TCPy Protein Binding

TCPy complexed with proteins found in cell culture medium and rat plasma. Over the range of concentrations tested, fraction of unbound TCPy ranged from 0.15 to 0.83, 0.13–0.89, and 0.47–0.81 in cell culture medium from the nonphysiological experiment, diluted plasma surrogate cell culture medium, and diluted rat plasma, respectively (Figure 3). Assuming one apparent-binding site (Equation 1), provided the best fit model for nonphysiological cell culture medium (BIC: 37.9 vs 41.5) and rat plasma (BIC: 37.5 vs 40.7), while the model assuming 2 binding sites (Equation 2) provided the best fit for plasma surrogate medium (BIC: 49.0 vs 66.7). The binding affinity constant (k_d) was lowest in the high affinity-binding site of the plasma surrogate medium (6.3 μM) and lowest in rat plasma (179 μM), indicating that TCPy has a higher binding affinity to albumin and proteins

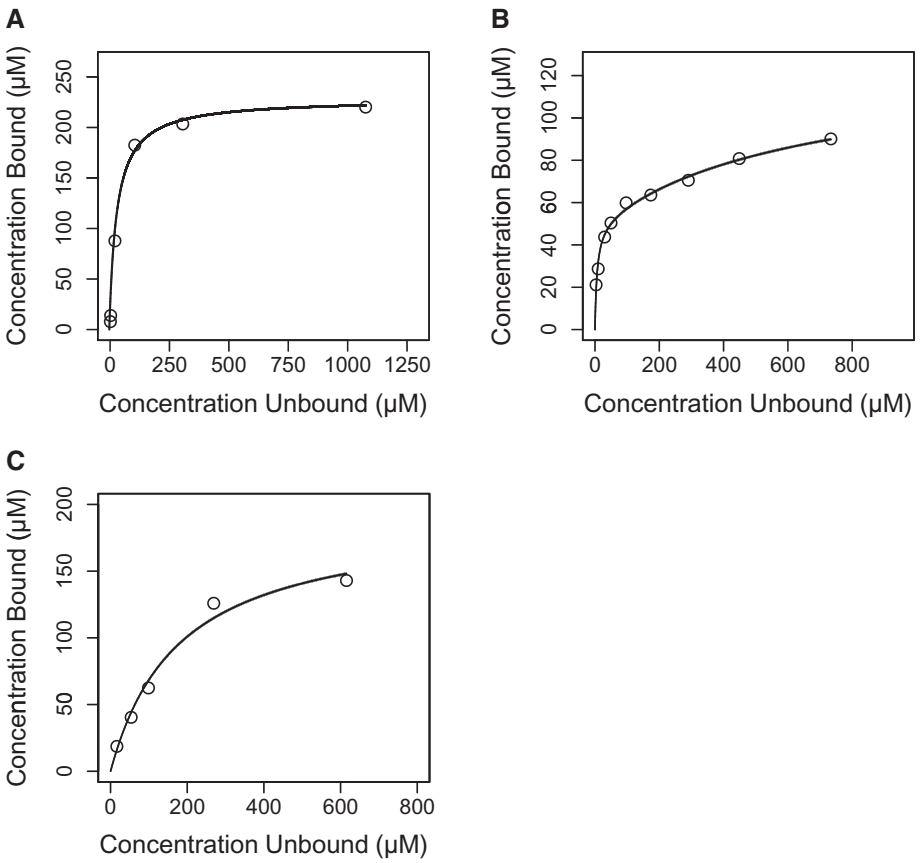

FIG. 3. Concentrations of TCPy bound and unbound to proteins in the cell culture medium from the nonphysiological experiment (**A**), diluted plasma surrogate cell culture medium from the physiological experiment (**B**), and diluted rat plasma (**C**). Lines in (A) and (C) are resulting fits to one-site model (Equation 1), while the line in Figure 3B is the resulting fit to a 2-site model (Equation 2).

in FBS compared with proteins in rat plasma. Measured B_{max} values were scaled by protein concentration when utilized in the PBPK and cellular transport computational models.

Tight Junctions

Tight junctions were maintained in serous-acinar monolayers throughout the nonphysiological and physiological transport experiments. TEER values of at least 1416 $\Omega \times cm^2$ were measured at the beginning and end of each experiment. Additionally, lucifer yellow transport was $\leq$ 0.48%/h and $\leq$ 0.09%/h for the durations of nonphysiological and physiological experiments, respectively. Physiological experiments had significantly lower lucifer yellow transport after 24 h compared with nonphysiological transport experiments (mean: 1.9% vs 3.5% of original level, *P* value: .03) suggesting that cellular permeability was more robust during the physiological transport experiments. In the physiological transport experiments, protein concentration gradients were maintained throughout the duration of the experiment. These 3 measurements (TEER, lucifer yellow and protein concentrations) indicate that integrity of the serous-acinar monolayers was robust and sustained over the course of each experiment for up to 32 h. Maintaining barrier function with tight junctions is critical for accurately measuring transport through the epithelial layer of cells.

Nonphysiological Transport Experiments

During nonphysiological experiments, TCPy demonstrated transport to equilibrium across the epithelial layer to equivalent concentrations in each chamber. After dosing the basolateral chamber (13–130 μM TCPy), TCPy was detectable by GC-MS as soon as 2-h postdosing in the apical chamber after all doses, and by 24 h, both chambers demonstrated equivalent TCPy concentrations under all nonphysiological transport experimental conditions (Figs. 4A–C). Additionally, mass balance of TCPy was maintained at each time point indicating that there was minimal loss of TCPy to metabolism, volatilization, or adhering to plastics used in the cell culture system. Equivalent equilibrium concentrations suggest passive diffusion as the primary transport mechanism, as an active polarized flux would lead to unequal concentrations at equilibrium with both chambers containing the same medium.

TCPy demonstrated dose-dependent times to reach equilibrium during nonphysiological transport experiments. TCPy concentrations in apical and basolateral chambers were statistically different until 24, 8, and 6 h ($P < .03$) for 13, 71, and 130 μM TCPy doses, respectively (Figs. 4A–C). Using protein binding parameters measured in cell culture medium with 2% FBS, the fraction of unbound TCPy is 0.12, 0.16, and 0.20 for those same TCPy doses, respectively. We hypothesize that this observation is evidence that unbound TCPy diffuses across the cell monolayer, while TCPy bound to proteins cannot. Increased levels of unbound TCPy leads to more rapid TCPy transport and reaching equilibrium more quickly. In combination, protein binding data and observations form the nonphysiological transport experiment suggest that protein binding is an important determinant in TCPy transport across cellular monolayers.

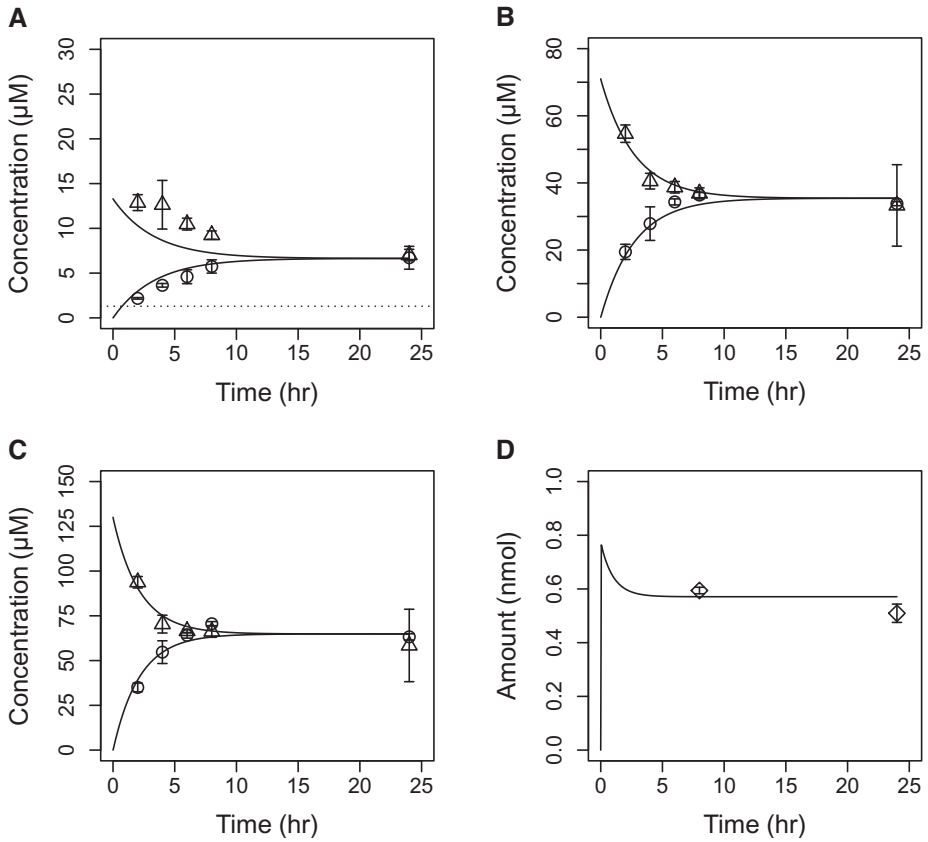

FIG. 4. Concentrations of TCPy in cell culture medium from apical (circles) and basolateral (triangles) chambers after the basolateral chamber was dosed with 13 (**A**), 71 (**B**), or 130 (**C**) μM of TCPy during nonphysiological transport experiments. TCPy amounts were measured in cells (diamonds) from a high dose experiment (140 μM) and was used to calculate the partition coefficient (**D**). Lines are cellular transport computational model fits to the data. The dotted line represents the limit of quantification (LOQ)

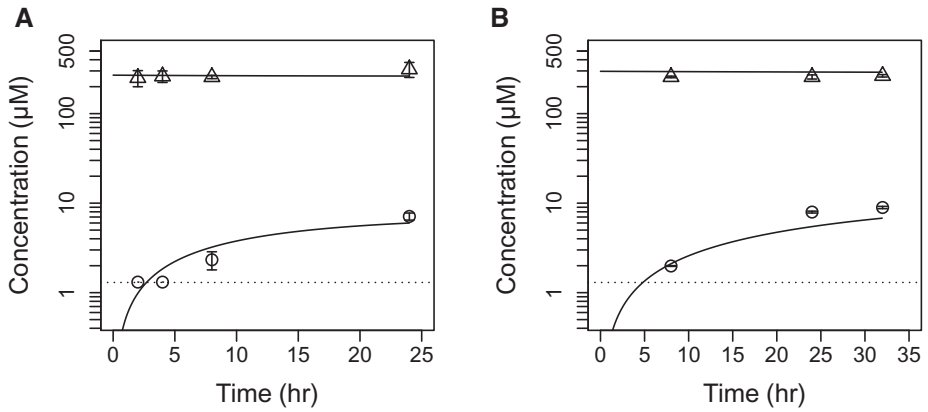

FIG. 5. Concentrations of TCPy in cell culture medium from apical (circles) and basolateral (triangles) chambers after the basolateral chamber was dosed with 269 (**A**) or 297 μM (**B**) TCPy during physiological transport experiments. TCPy transport was consistent across relative (**A**) and absolute (**B**) physiological protein levels. Lines are cellular transport computational model fits to the data. The dotted line represents the LOQ.

The cellular transport computational model was parameterized using literature, measured, and optimized parameters. Many parameters were defined by nonphysiological transport experiments (eg, chamber volumes, cellular surface area) (Table 1). B_{max} values were extrapolated from corresponding protein-binding experiments using a total protein basis. The second order k_{on} rate constant (1×10^6 1/M/s) was estimated based on literature values of small molecules binding to proteins limited by diffusion assuming protein conformational changes are not necessary to facilitate TCPy binding (Mironov *et al.*, 2011; Schlosshauer and Baker, 2004; Schreiber *et al.*, 2009). First order k_{off} rate constants were calculated ($k_d \times k_{on}$). Unbound TCPy cellular partitioning was measured in the high dose nonphysiological transport experiment. The permeation coefficient was optimized to TCPy concentrations in apical and basolateral chambers following a 71 μM TCPy dose (Figure 4B).

TABLE 2. Parameters Used in the PBPK Model Simulating TCPy Transport into Rat Saliva

Parameter	Value	References
Rat Parameters		
Blood flow to salivary tissues (fraction cardiac output)	0.002	Hiramatsu *et al.* (1994)
Salivary tissue volume (fraction body weight)	0.00116	Human, ICRP (2002)
Volume of blood in salivary glands (fraction body weight)	0.0005	Estimated based on thyroid, gonad, and adrenal in humans (ICRP, 2002)
Capilary surface area in salivary tissues (cm^2/g tissue)	512	Clough and Smaje (1984)
Permeation coeffcient (cm/h)	0.41	Optimized from physiological transport experiment
$P_{unbound\ in\ media:cells}$ TCPy	24	Measured in standard transport experiment
B_{max} (nmol/mg protein)	108.7	Measured
K_d (μM)	179.1	Measured
Plasma protein (mg/ml)	62.1	Measured

After parameterization, the cellular transport computational model was able to reasonably simulate nonphysiological transport experiments at all TCPy dose levels. The model accurately predicted TCPy concentrations in both chambers from the 2 high TCPy doses (Figs. 4B and C) and TCPy levels in cells from the high dose (Figure 4D). In the low dose, mean TCPy concentrations in the basolateral chamber (which had 5%–20% variability) were under predicted (20%–30%), and TCPy concentrations in the apical chamber were slightly over predicted by a similar magnitude, indicating the model is slightly under predicting transport for this concentration. As observed from the experimental data, the model predicted dose-dependent times to reach equilibrium. TCPy concentrations reached equilibrium faster following the high dose compared with the low dose as chamber concentrations were within 1% at 11.3 versus 17.7 h, respectively. Overall, the cellular transport computational model was able to reasonably simulate nonphysiological transport experiments after optimizing the permeation coefficient.

Physiological Transport Experiments

TCPy transport in the physiological experiments was much slower than those from the nonphysiological experiments, and equilibrium was achieved with different concentrations in the 2 chambers. After dosing TCPy into the basolateral chamber (270–300 μM), TCPy was first observed in the apical side 8 h after dosing (Figure 5). Equilibrium was achieved at 24+ h (Figure 5B), and TCPy concentrations in the basolateral chamber (plasma surrogate) were significantly higher than those in the apical chamber (saliva surrogate) (Figure 5). At equilibrium, the TCPy concentration ratio of apical to basolateral chambers was 0.034. We hypothesize that slower transport rates and higher TCPy levels in the basolateral chamber are due to high levels of TCPy binding to proteins which are unable to transverse the cellular monolayer.

The cellular transport computational model was able to simulate data from physiological transport experiments after reoptimizing the permeation coefficient. After adjusting B_{max} and k_d values measured in protein binding experiments (Table 1) and maintaining all other parameters from nonphysiological transport experiments, the cellular transport computational model overestimated TCPy concentrations in the apical chamber during the first measurable time points (approximately 2.5× at 8 h) from physiological transport experiments (data not shown) but fit later time points (≥24 h). The permeation coefficient was reoptimized using data from the 24 h physiological transport experiment (Figure 5A), and resulting simulations predicted physiological transport data reasonably well (Figure 5).

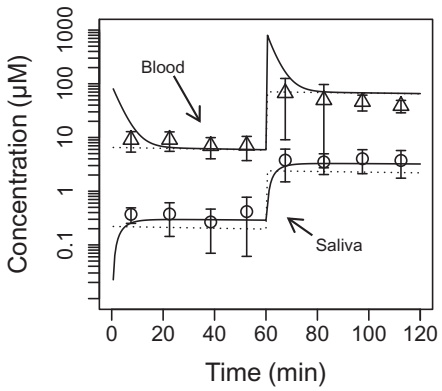

FIG. 6. TCPy concentrations in blood (triangles) and saliva (circles) from rats being progressively dosed with 1 mg/kg TCPy at 0 min and 10 mg/kg TCPy at 60 min (Smith *et al.*, 2010). The solid line is the modified PBPK model simulation using the protein-binding model descripted here (Figure 2). The dotted line is the historical PBPK model simulation using 0.034 as the saliva:blood ratio measured in the physiological transport experiment. Note: concentration is on a logarithmic scale.

The reoptimized physiological permeation coefficient was approximately 2.5× lower than the nonphysiological permeation coefficient (0.41 vs 1.14, respectively), suggesting that increased protein level may have reduced cellular permeability. This data is consistent with lower levels of lucifer yellow transport observed in the same experiments (see "Tight Junctions" section). TCPy concentrations in media containing both absolute and relative protein levels were accurately simulated by one common set of parameters (with the exception of B_{max}), suggesting that both conditions resulted in consistent TCPy transport.

In Vivo *Extrapolation*

The cellular transport computational model was integrated into a PBPK model for chlorpyrifos to assess its ability to extrapolate from the *in vitro* serous-acinar assay to measured TCPy levels in saliva of rats (Smith *et al.*, 2010, 2012). The previous description of TCPy disposition was adapted to be more compatible with the cellular transport computational model developed here (Figure 2) while maintaining fidelity with the original chlorpyrifos PBPK model (Timchalk *et al.*, 2002). Parameters were adapted from the previous model, literature sources, protein binding measurements, and transport experiments conducted here (Table 2). The slower physiological permeation coefficient was

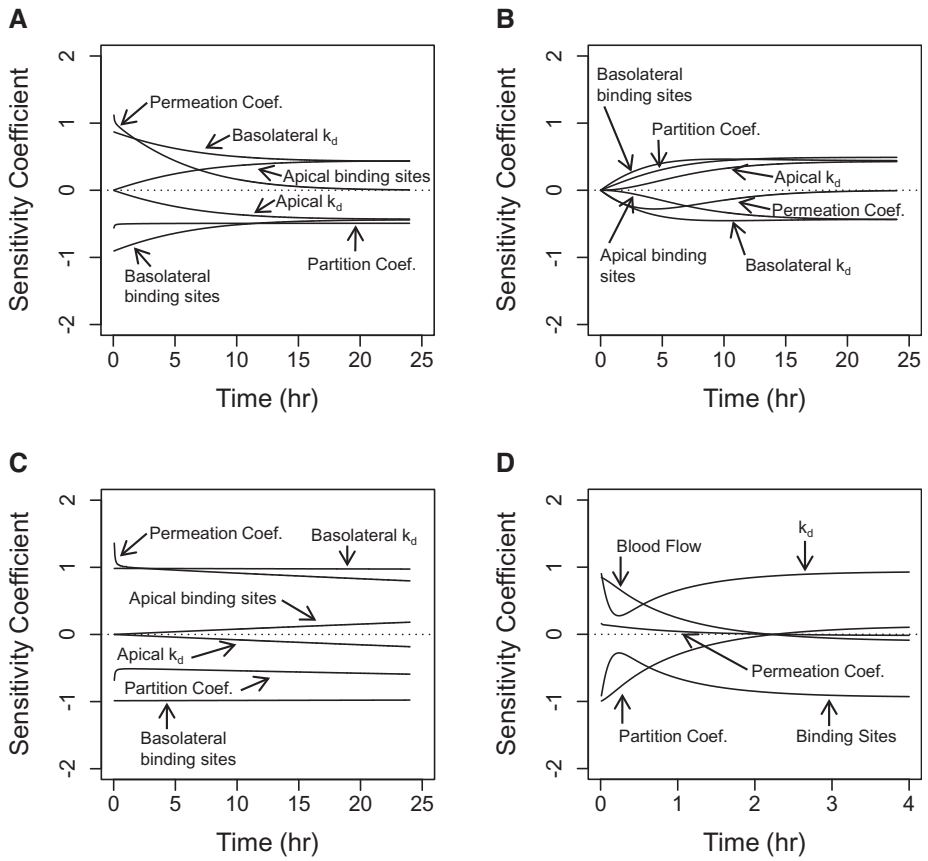

FIG. 7. Sensitivity coefficients of selected model parameters over time. Simulations include nonphysiological transport experiment in respect to TCPy concentrations in the apical (A) and basolateral (B) chambers, physiological transport experiment in respect to TCPy concentrations in the apical chamber (C), and iv administration (1 mg/kg) of TCPy to rats in respect to TCPy concentrations in saliva (D). For *in vitro* simulations (A–C), the starting TCPy concentration in the basolateral chamber was 10 μM.

utilized in the PBPK model, as we assumed that experiment had greater physiological relevance.

The modified PBPK model based on protein binding and permeation coefficient measured here was able to predict TCPy concentrations in rat saliva following TCPy administration (Figure 6). In a previous study, double cannulated rats were infused with pilocarpine to stimulate salivation and were progressively dosed iv with 1 mg/kg TCPy at 0 min and 10 mg/kg TCPy at 60 min (Smith *et al.*, 2010). Utilizing the measured saliva:blood partition coefficient from the physiological transport experiment, the previous PBPK model (Smith *et al.*, 2010) was able to accurately predict TCPy concentrations in blood and saliva from these rats (Figure 6). The modified PBPK model based on protein binding and permeation coefficient measured here also was able to accurately predict TCPy concentrations in saliva and blood, while slightly over predicting blood concentrations at 7.5 min postdosing (Figure 6). This phase of TCPy distribution is driven by protein binding in plasma (see "Sensitivity Analysis" section), and further model refinement may be necessary for higher model accuracy at very early time points (<10 min). Overall, this experimental and computational strategy demonstrates *in vitro* to *in vivo* extrapolation of TCPy transport in saliva.

Sensitivity Analysis

Sensitivity analyses identified which parameters are most important for model output under different experimental scenarios using the cellular transport computational model and the PBPK model. For the cellular transport computational model, permeation coefficients and protein-binding coefficients in the basolateral chamber were the most sensitive parameters from simulations of nonphysiological (Figure 7A) and physiological transport experiments (Figure 7C) in respect to TCPy concentrations in the apical (nondosing) chamber. In both simulations (10 μM starting TCPy concentration in the basolateral chamber), the permeation coefficient was the most sensitive parameter during the earliest time points (Figs. 7A and C). Basolateral chamber binding parameters (k_d and binding sites) were also sensitive, especially during early time points of the nonphysiological transport simulation (Figure 7A). In the physiological transport simulation, sensitivities of the permeation coefficient and basolateral-binding parameters were much more consistent over the simulation time course (Figure 7C). In both simulations, sensitivity of apical binding parameters increased with time and was more sensitive in the nonphysiological transport simulation. A higher TCPy starting concentration (100 μM) resulted in no demonstrative differences in parameter sensitivities (data not shown). For the nonphysiological experiment in respect to the basolateral (dosing) chamber, basolateral binding parameters were among the most sensitive throughout the simulation time course (Figure 7B). In early time points (<10 h), permeation coefficients were also important, and in later time points (>5 h), the partition coefficient and apical-binding parameters gained importance (Figure 7B).

For the physiological experiment in respect to the basolateral (dosing) chamber, essentially all parameters were insensitive (data not shown), which is unsurprising, as TCPy concentrations in the basolateral chamber remained relatively static over the time course of the simulation (Figure 5). Overall, permeation coefficients and protein binding coefficients in the basolateral chamber were most consistently important in the cellular transport computational model, especially in respect to TCPy concentrations in the apical chamber.

Sensitivity analysis of parameters extrapolated from the cellular transport computational model to the PBPK model was also conducted. In early time points (<45 min), blood flow and partition coefficients were the most sensitive extrapolated parameters in respect to TCPy concentrations in saliva (Figure 7D). At later time points (>45 min), plasma binding parameters were dominant (Figure 7D). The permeation coefficient was not a sensitive parameter under these simulation conditions (Figure 7D). This suggests that although differences permeation coefficient were measured in the nonphysiological and physiological *in vitro* experiments, implications of selecting either parameter for *in vivo* extrapolation are small, and protein binding parameters are more import under these simulation conditions. Of parameters extrapolated from the cellular transport computational model, only plasma protein binding parameters were sensitive <0.5 h in respect to TCPy concentration in blood (data not shown), suggesting that saliva is not a major clearance route for TCPy. Overall, plasma protein-binding parameters were most important for TCPy transport to saliva under these simulation conditions.

DISCUSSION

Predicting which chemicals and the extent they are detectable in saliva remains a challenge for salivary biomonitoring. An experimental and computational approach to predict chemical transport into saliva for biomonitoring was developed here and demonstrated using TCPy, a metabolite of the pesticide chlorpyrifos. TCPy protein binding and transport during nonphysiological and physiological based experiments with serous-acinar cells were measured. A cellular transport model was developed and adapted to a PBPK model, which was used to predict TCPy transport in the cellular experiments and TCPy concentrations in saliva of rats administered TCPy, respectively.

To our knowledge, this is the first time this approach has been applied to salivary transport. Others have used cellular based systems, such as Caco-2 cells and Madin–Darby canine kidney (MDCK) cells, to measure chemical and drug permeation in cells (Balimane and Chong, 2005; Irvine *et al.*, 1999; Volpe, 2008, 2011). Others have applied computational modeling approaches to cellular chemical transport assays (Poirier *et al.*, 2008). However, a combination approach has not been readily applied, especially to chemical transport in saliva.

When protein binding is considered, cellular permeability of serous-acinar are similar to the more commonly used Caco-2 cells. Apparent permeability coefficients for small molecule Caco-2 transport generally range from 0.004 to 0.4 cm/h (Yee, 1997). Here we measured unbound TCPy permeability coefficients measured here were 0.4 and 1.4 cm/h for physiological and nonphysiological experiments, respectively. These values are not completely comparable, as reported permeation coefficients (Yee, 1997) do not take into consideration protein binding. Thus, it is expected that permeation coefficients for unbound compounds would increase if protein binding is significant. If protein binding is trivial for reported compounds, Caco-2 may have similar permeability properties to serous-acinar monolayers under physiologically relevant conditions.

Unlike the cellular transport computational model, which had descriptions of protein binding in all media compartments, the PBPK model of salivary transport did not have protein-binding descriptions in the saliva compartment for 2 primary reasons. First, apical-binding parameters were not sensitive in physiological transport simulations, especially at early time points. This suggests that additional complexity of salivary protein binding in the PBPK model would add little in terms of predictive capability. Second, *in vivo* saliva is constantly flowing, whereas in the serous-acinar chemical transport assay, the apical chamber is static. Flowing saliva would further reduce the sensitivity of salivary binding parameters as the time required for binding parameters to gain significant sensitivity is slow compared with the salivary flow rate. These assumptions are all based on TCPy measured and optimized parameters and should be evaluated for other chemicals.

In this study, we observed that by utilizing a cellular system that is more representative of physiology in terms of protein levels, we were able to more accurately predict actual TCPy levels observed in rat saliva. The TCPy saliva:plasma ratios have been previously measured at 0.049 after TCPy administration (Smith *et al.*, 2010) and 0.055 after chlorpyrifos administration (Smith *et al.*, 2012). These values are comparable to the observed physiological ratio here (0.034) but significantly different from that observed in the nonphysiological transport experiment (1), suggesting more physiologically representative experiments are better predictors of the real world. Although this conclusion may seem fairly obvious, increased physiological relevance is not always considered during *in vitro* toxicology experiments. For example, there are few cellular metabolism and transport studies conducted using protein concentrations in cell culture medium equivalent to those in plasma. Implications of physiological levels of protein binding could range from insignificant to substantial depending on the chemical, level of protein binding for that chemical, and the assay conducted (Poulin *et al.*, 2012, 2016; Schmidt *et al.*, 2010; Zeitlinger *et al.*, 2011).

Increased protein levels have shown the ability to alter cellular permeability. Here, we observed a reduction of cellular permeability to TCPy and lucifer yellow with increased protein levels (mostly bovine serum albumin). Other studies have also observed reduced cellular permeability in response to higher levels of albumin including cell models (Lum *et al.*, 1991), isolated perfused tissues (McDonagh, 1983), and rodent models (Schneeberger and Hamelin, 1984; Wang *et al.*, 2007). These observations have led some to hypothesize that albumin plays a critical role in regulating endothelial barriers (Lum *et al.*, 1991; McDonagh, 1983; Wang *et al.*, 2007), and albumin may be playing a similar role in reducing permeability of salivary gland epithelial cells observed here. Alternatively, osmolality of the system is also being altered which could induce “swelling” of cells, enhance tight junctions, and reduce permeability. Further experiments are needed to elucidate a mechanism.

Even though the physiological transport experiment may have better *in vivo* predictive capability than the nonphysiological transport experiment, the nonphysiological transport experiment still has utility for investigating transport mechanisms. The observation that TCPy concentrations in apical and basolateral chambers reached a common equilibrium concentration suggests that there are no active polarized flux. This observation could not have been reached from the physiological transport data alone, and we recommend that both types of

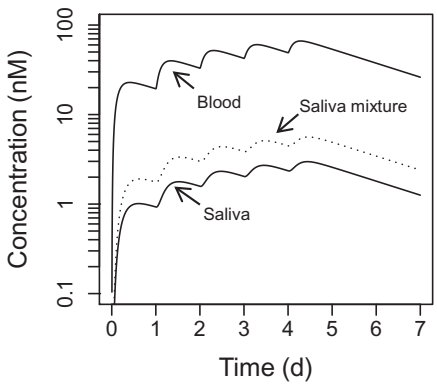

FIG. 8. Predicted TCPy concentrations in blood and saliva of humans exposed to 3 μg/kg/d of chlorpyrifos for 5 days using a modified PBPK model developed here. The dotted line represents the same simulation in a chemical mixture, where other chemicals could compete for binding sites with TCPy. To simulate this scenario, the number of binding sites was reduced by 50%. Note: concentration is on a logarithmic scale.

experiments should be utilized when transport mechanisms are unknown.

Although some species differences exist, the salivary system between rats and humans is fairly similar. Three primary glands (parotid, submandibular, and sublingual) and several minor glands contribute to mixed saliva (serous and mucoidal saliva) in both species. One major difference between the 2 species is in the submandibular gland, where in rats, both serous and mucoidal type cells make up the gland, while in humans, only serous cells are present (Amano *et al.*, 2012). Here, serous cells from rat submandibular glands were cultured and used to measure TCPy transport. Using a cell type that is common between species should increase the utility of this cellular model for species extrapolation.

Species-specific parameters for extrapolating physiology of salivary glands are rare in the literature. This observation was made nearly 20 years ago (Smaje, 1998) and still persists today. As such, many parameters utilized here were shared across species. For example, fraction of tissue volumes and fraction of blood volume within tissues (estimated from other tissues) were obtained from humans, while fraction of cardiac output was from rats, and relative surface area of blood vessels were from rabbits (Table 2). These parameters were scaled by species-specific values (eg, cardiac output from rat or human); however, the overall physiology utilized is a various blend of 3 species. Implications of this mixed species physiology on predicting salivary transports are unknown; however, sensitivity analyses can guide to which parameters are important. Sensitivity analyses on simulations of TCPy in rat saliva indicate that blood flow to saliva gland, protein-binding parameters, and partition coefficient are important (Figure 6D). Among these parameters, TCPy protein-binding parameters in human plasma are probably the next data need for future focus.

Humans are rarely exposed to single chemicals and are instead typically exposed to a mixture of various chemicals, which could lead to interesting implications regarding salivary transport. It is plausible that exposure to a mixture of chemicals could create competition for protein-binding sites especially if several chemicals share binding sites and binding sites are limited. This scenario could result in higher levels of unbound compound and enhanced salivary clearance. To explore this possibility, the PBPK model was extrapolated to humans using parameters measured here. The oral reference dose of chlorpyrifos (3 μg/kg/d) was simulated for 5 consecutive days, and the model predicts TCPy concentrations in saliva at approximately 2 nM for this scenario (Figure 8). A chemical mixture coexposure was simulated by reducing the number of binding sites by 50%, assuming that other chemicals would limit binding sites available for TCPy thorough competition. Under this scenario, TCPy levels in saliva are predicted to roughly double compared with a single chemical exposure due to increased unbound TCPy levels in blood (Figure 8). This suggests that exposure to chemical mixtures may have significant implications on salivary transport of highly bound chemicals through competitive binding and could be partially responsible for high levels of variability sometimes observed in saliva:blood ratios (Michalke *et al.*, 2015). Further experiments to test this hypothesis include protein-binding evaluations and appropriate physiological transport experiments.

In conclusion, we developed an experimental and computational approach to evaluate and predict chemical transport in saliva. TCPy complexed with proteins found in cell culture medium and rat plasma, and high levels of protein binding resulted in different transport behaviors observed from nonphysiological and physiological transport experiments utilizing protein and salivary surrogates for cell culture medium. In the nonphysiological transport experiment, the time required for TCPy concentrations to reach equilibrium decreased in dose-dependent manner, and equilibrium was achieved at equivalent concentrations. In the physiological experiment, TCPy transport was slower, and equilibrium was achieved with different concentrations at a ratio (0.034) comparable to previously measured saliva:blood TCPy ratio in rats (0.049). A cellular transport computational model was developed and simulated transport experiments reasonably well using different permeability coefficients for type of experiment (1.4 and 0.4 cm/h for nonphysiological and physiological transport experiments, respectively). The computational model was integrated into an existing PBPK model which was able to accurately predict TCPy concentrations in saliva of rats dosed with TCPy. Overall, this approach demonstrates the utility of a combination experimental and computational approach to predict chemical transport in saliva, potentially increasing the utility of salivary biomonitoring in the future.

FUNDING

This work was supported by Centers for Disease Control and Prevention/The National Institute for Occupational Safety and Health (CDC/NIOSH) grants R01 OH008173 and R01 OH011023.

REFERENCES

Amano, O., Mizobe, K., Bando, Y., and Sakiyama, K. (2012). Anatomy and histology of rodent and human major salivary glands: -overview of the Japan salivary gland society-sponsored workshop. *Acta Histochem. Cytochem.* **45**, 241–250.

Balimane, P. V., and Chong, S. (2005). Cell culture-based models for intestinal permeability: A critique. *Drug Discov. Today* **10**, 335–343.

Brzak, K. A., Harms, D. W., Bartels, M. J., and Nolan, R. J. (1998). Determination of chlorpyrifos, chlorpyrifos oxon, and 3,5,6-

trichloro-2-pyridinol in rat and human blood. *J. Anal. Toxicol.* **22**, 203–210.

Clough, G., and Smaje, L. H. (1984). Exchange area and surface properties of the microvasculature of the rabbit submandibular gland following duct ligation. *J. Physiol.* **354**, 445–456.

Haeckel, R. (1993). Factors influencing the saliva/plasma ratio of drugs. *Ann. N. Y. Acad. Sci.* **694**, 128–142.

Hiramatsu, Y., Nagler, R. M., Fox, P. C., and Baum, B. J. (1994). Rat salivary gland blood flow and blood-to-tissue partition coefficients following X-irradiation. *Arch. Oral Biol.* **39**, 77–80.

Hold, K. M., de Boer, D., Zuidema, J., and Maes, R. A. A. (1995). Saliva as an analytical tool in toxicology. *Int. J. Drug Test* **1**, 1–36.

ICRP. (2002). Basic anatomical and physiological data for use in radiological protection reference values. ICRP Publication 89. *Ann. ICRP* **32**.

Irvine, J. D., Takahashi, L., Lockhart, K., Cheong, J., Tolan, J. W., Selick, H. E., and Grove, J. R. (1999). MDCK (Madin-Darby canine kidney) cells: A tool for membrane permeability screening. *J. Pharm. Sci.* **88**, 28–33.

Jusko, W. J., and Milsap, R. L. (1993). Pharmacokinetic principles of drug distribution in saliva. *Ann. N. Y. Acad. Sci.* **694**, 36–47.

Kaufman, E., and Lamster, I. B. (2002). The diagnostic applications of saliva—A review. *Crit. Rev. Oral Biol. Med.* **13**, 197–212.

Lu, C., Anderson, L. C., and Fenske, R. A. (1997). Determination of atrazine levels in whole saliva and plasma in rats: Potential of salivary monitoring for occupational exposure. *J. Toxicol. Environ. Health* **50**, 101–111.

Lu, C., Irish, R. M., and Fenske, R. (2003). Biological monitoring of diazinon exposure using saliva in an animal model. *J. Toxicol. Environ. Health A* **66**, 2315–2325.

Lum, H., Siflinger-Birnboim, A., Blumenstock, F., and Malik, A. B. (1991). Serum albumin decreases transendothelial permeability to macromolecules. *Microvasc Res.* **42**, 91–102.

McDonagh, P. F. (1983). Both protein and blood cells reduce coronary microvascular permeability to macromolecules. *Am. J. Physiol.* **245**, H698–H706.

Michalke, B., Rossbach, B., Goen, T., Schaferhenrich, A., and Scherer, G. (2015). Saliva as a matrix for human biomonitoring in occupational and environmental medicine. *Int. Arch. Occup. Environ. Health* **88**, 1–44.

Mironov, G. G., Okhonin, V., Gorelsky, S. I., and Berezovski, M. V. (2011). Revealing equilibrium and rate constants of weak and fast noncovalent interactions. *Anal. Chem.* **83**, 2364–2370.

National Research Council. (2012). In Exposure Science in the 21st Century: A Vision and a Strategy. Washington, DC: The National Academies Press. doi: https://doi.org/10.17226/13507.

Nieuwenhuijsen, M., Paustenbach, D., and Duarte-Davidson, R. (2006). New developments in exposure assessment: The impact on the practice of health risk assessment and epidemiological studies. *Environ. Int.* **32**, 996–1009.

Nigg, H. N., and Wade, S. E. (1992). Saliva as a monitoring medium for chemicals. *Rev. Environ. Contam. Toxicol.* **129**, 95–119.

Poirier, A., Lave, T., Portmann, R., Brun, M. E., Senner, F., Kansy, M., Grimm, H. P., and Funk, C. (2008). Design, data analysis, and simulation of in vitro drug transport kinetic experiments using a mechanistic in vitro model. *Drug Metab. Dispos.* **36**, 2434–2444.

Poulin, P., Burczynski, F. J., and Haddad, S. (2016). The role of extracellular binding proteins in the cellular uptake of drugs: Impact on quantitative in vitro-to-in vivo extrapolations of toxicity and efficacy in physiologically based pharmacokinetic-pharmacodynamic research. *J. Pharm. Sci.* **105**, 497–508.

Poulin, P., Kenny, J. R., Hop, C. E., and Haddad, S. (2012). In vitro-in vivo extrapolation of clearance: Modeling hepatic metabolic clearance of highly bound drugs and comparative assessment with existing calculation methods. *J. Pharm. Sci.* **101**, 838–851.

Ritschel, W. A., and Tompson, G. A. (1983). Monitoring of drug concentrations in saliva: A non-invasive pharmacokinetic procedure. *Methods Find Exp. Clin. Pharmacol.* **5**, 511–525.

Schlosshauer, M., and Baker, D. (2004). Realistic protein-protein association rates from a simple diffusional model neglecting long-range interactions, free energy barriers, and landscape ruggedness. *Protein Sci.* **13**, 1660–1669.

Schmidt, S., Gonzalez, D., and Derendorf, H. (2010). Significance of protein binding in pharmacokinetics and pharmacodynamics. *J. Pharm. Sci.* **99**, 1107–1122.

Schmitt, W. (2008). General approach for the calculation of tissue to plasma partition coefficients. *Toxicol. In Vitro* **22**, 457–467.

Schneeberger, E. E., and Hamelin, M. (1984). Interaction of serum proteins with lung endothelial glycocalyx: Its effect on endothelial permeability. *Am. J. Physiol.* **247(2 Pt 2)**, H206–H217.

Schreiber, G., Haran, G., and Zhou, H. X. (2009). Fundamental aspects of protein-protein association kinetics. *Chem. Rev.* **109**, 839–860.

Smaje, L. H. (1998). Capillary dynamics in salivary glands. In *Glandular Mechanisms of Salivary Secretion* (J. R. Garrett, J. Ekstrom, and L. C. Anderson, Eds.), Vol. **10**, pp. 118–131. Karger, Basel, Switzerland.

Smith, J. N., Wang, J., Lin, Y., Klohe, E. M., and Timchalk, C. (2012). Pharmacokinetics and pharmacodynamics of chlorpyrifos and 3,5,6-trichloro-2-pyridinol in rat saliva after chlorpyrifos administration. *Toxicol. Sci.* **130**, 245–256.

Smith, J. N., Wang, J., Lin, Y., and Timchalk, C. (2010). Pharmacokinetics of the chlorpyrifos metabolite 3,5,6-trichloro-2-pyridinol (TCPy) in rat saliva. *Toxicol. Sci.* **113**, 315–325.

Teeguarden, J. G., Tan, Y. M., Edwards, S. W., Leonard, J. A., Anderson, K. A., Corley, R. A., Kile, M. L., S., L. M. S., Stone, D., Tanguay, R. L., *et al.* (2016). Expanding on Successful Concepts, Models, and Organization. *Environ. Sci. Technol.* **50**, 8921–8922.

Timchalk, C., Campbell, J. A., Liu, G., Lin, Y., and Kousba, A. A. (2007). Development of a non-invasive biomonitoring approach to determine exposure to the organophosphorus insecticide chlorpyrifos in rat saliva. *Toxicol. Appl. Pharmacol.* **219**, 217–225.

Timchalk, C., Nolan, R. J., Mendrala, A. L., Dittenber, D. A., Brzak, K. A., and Mattsson, J. L. (2002). A Physiologically based pharmacokinetic and pharmacodynamic (PBPK/PD) model for the organophosphate insecticide chlorpyrifos in rats and humans. *Toxicol. Sci.* **66**, 34–53.

Timchalk, C., Weber, T. J., and Smith, J. N. (2015). Computational strategy for quantifying human pesticide exposure based upon a saliva measurement. *Front. Pharmacol.* **6**, 115.

Volpe, D. A. (2011). Drug-permeability and transporter assays in Caco-2 and MDCK cell lines. *Future Med. Chem.* **3**, 2063–2077.

Volpe, D. A. (2008). Variability in Caco-2 and MDCK cell-based intestinal permeability assays. *J. Pharm. Sci.* **97**, 712–725.

Wang, R., Ashwal, S., Tone, B., Tian, H. R., Badaut, J., Rasmussen, A., and Obenaus, A. (2007). Albumin reduces blood-brain barrier permeability but does not alter infarct size in a rat model of neonatal stroke. *Pediatr. Res.* **62**, 261–266.

Weber, T. J., Smith, J. N., Carver, Z. A., and Timchalk, C. (2017). Non-invasive saliva human biomonitoring: Development of an in vitro platform. *J. Expo. Sci. Environ. Epidemiol.* **27**(1), 72–77.

Yee, S. (1997). In vitro permeability across Caco-2 cells (colonic) can predict in vivo (small intestinal) absorption in man–fact or myth. *Pharm. Res.* **14**, 763–766.

Zaias, J., Mineau, M., Cray, C., Yoon, D., and Altman, N. H. (2009). Reference values for serum proteins of common laboratory rodent strains. *J. Am. Assoc. Lab. Anim. Sci.* **48**, 387–390.

Zeitlinger, M. A., Derendorf, H., Mouton, J. W., Cars, O., Craig, W. A., Andes, D., and Theuretzbacher, U. (2011). Protein binding: Do we ever learn? *Antimicrob. Agents Chemother.* **55**, 3067–3074.